

## Analyses of airborne $^7\text{Be}$ concentrations in Hong Kong using back-trajectories

L.Y.L. Lee<sup>a</sup>, R.C.W. Kwok<sup>b</sup>, Y.P. Cheung<sup>a</sup>, K.N. Yu<sup>a,\*</sup>

<sup>a</sup>Department of Physics and Materials Science, City University of Hong Kong, Tat Chee Avenue, Kowloon Tong, Hong Kong

<sup>b</sup>Department of Public and Social Administration, City University of Hong Kong, Tat Chee Avenue, Kowloon Tong, Hong Kong

Received 20 September 2003; received in revised form 3 November 2003; accepted 12 November 2003

### Abstract

A total of 71 air samples were collected in Hong Kong area from November 2001 to February 2003 using a high-volume air sampler and a high-volume cascade impactor with five atmospheric pressure stages. The  $^7\text{Be}$  radioactivity on each stage was measured using a high-efficiency germanium gamma-ray spectrometer. From the radioactivity of stages, the total airborne  $^7\text{Be}$  radioactivity was determined. The activity median aerodynamic diameter (AMAD) of  $^7\text{Be}$ -associated atmospheric aerosols was found to be 0.22–1.11  $\mu\text{m}$  and the geometric standard deviation (GSD) was found to be 1.2–10.5. With the assumed mean growth rate (MGR) of atmospheric aerosols of 0.004–0.005  $\mu\text{m h}^{-1}$  and the size of Aitken nuclei of 0.015  $\mu\text{m}$ , the residence times of  $^7\text{Be}$ -associated atmospheric aerosols were also found from the AMAD.

Three-dimensional 4-day back-trajectories were obtained using the HYSPLIT model from NOAA Air Resources Laboratory. These trajectories were used with the measured  $^7\text{Be}$  radioactivity to construct regional  $^7\text{Be}$  intensity fields for four different altitude levels (less than 1000, 1000–2000, 2000–3000 and above 3000 m) with a Geographic Information System (GIS). Low  $^7\text{Be}$  intensities were found to have advected from low altitudes (less than 1000 m) and oceanic areas. The  $^7\text{Be}$  intensities increased for the higher intensity field layers.

By comparing the time taken for air masses to come from the  $^7\text{Be}$  source to Hong Kong and the residence time determined from the AMAD of  $^7\text{Be}$ -associated atmospheric aerosols, good agreement was found if the mean growth rate of 0.005  $\mu\text{m h}^{-1}$  for atmospheric aerosols was used, and the use of back-trajectories was shown to be satisfactory even up to about 6.5 d. By using the residence time with a MGR of 0.005  $\mu\text{m h}^{-1}$ , the  $^7\text{Be}$  source was found to be relatively well confined in the areas of Mongolia and southeastern Siberia, which further supported that the association of  $^7\text{Be}$  source with the Siberian anticyclone.

© 2004 Elsevier Ltd. All rights reserved.

**Keywords:**  $^7\text{Be}$ ; AMAD; Residence time; Back-trajectories; HYSPLIT; Geographic Information System; Anticyclone

### 1. Introduction

The cosmogenic radionuclide  $^7\text{Be}$  is formed by spallation processes of light atmospheric nuclei such as carbon ( $Z = 6$ ), nitrogen ( $Z = 7$ ) and oxygen ( $Z = 8$ ), when they absorb protons and even neutrons of the primary component of cosmic rays. It can reach the

\*Corresponding author. Tel.: +852 2788 7812; fax: +852 2788 7830.

E-mail address: peter.yu@cityu.edu.hk (K.N. Yu).

ground level through vertical mixing in the troposphere. It emits gamma rays of energy 477.6 keV, and has a half-life of 53.3 d or equivalently an average lifetime of 77 d, and has been employed to study aerosol transit and residence times in the troposphere (Martell, 1970; Papastefanou and Ioannidou, 1995).

Atmospheric aerosol particles, in general, follow a trimodal distribution including (a) the Aitken nuclei mode (from 0.003 to 0.07  $\mu\text{m}$ , average 0.015  $\mu\text{m}$ ), (b) the accumulation mode (from 0.07 to 2  $\mu\text{m}$ , average 0.3  $\mu\text{m}$ ), and (c) the coarse mode (from 2 to 36  $\mu\text{m}$ , average >10  $\mu\text{m}$ ) (NRC 1979). However,  $^7\text{Be}$  associates mainly with the accumulation-mode aerosols (Papastefanou and Ioannidou, 1995). After attachment, the transportation and deposition characteristics of  $^7\text{Be}$  become those of the aerosol particles, so  $^7\text{Be}$  is a good tracer for the characteristics of the accumulation mode aerosols.

Studies of the  $^7\text{Be}$  concentrations have been carried out at different places (e.g. Papastefanou and Ioannidou, 1995; Takayuki et al., 1996; El-Hussein et al., 2001; Gerasopoulos et al., 2001). Most  $^7\text{Be}$  resides in the stratosphere. Feely et al. (1989) states that its production rate is the greatest in the upper stratosphere, and decreases with the altitude down to ground level. Therefore, many studies (e.g. Stohl et al., 2000) use it to indicate the phenomenon of stratosphere-to-troposphere exchange (STE).

Two  $^7\text{Be}$  physical characteristics were experimentally measured or derived in the present work. The first physical characteristic was the airborne  $^7\text{Be}$  radioactivity. The second physical characteristic was the activity median aerodynamic diameter (AMAD) derived from the aerodynamic size distribution of  $^7\text{Be}$ -associated atmospheric aerosols. From the AMAD, the residence time of the aerosols were also determined. It is noted that, in the literature, there are many more studies on  $^7\text{Be}$  concentrations (e.g., Papastefanou et al., 1995; Talpos and Cuculeanu, 1997; Todorovic et al., 1999; Al-Azmi et al., 2001; Aldahan et al., 2001; El-Hussein et al., 2001; Gerasopoulos et al., 2001) than on  $^7\text{Be}$  size distribution (Papastefanou and Ioannidou, 1995; Winkler et al., 1998; Yu and Lee, 2002).

The first objective of the present work was to analyze the measured  $^7\text{Be}$  radioactivity using back-trajectories. A method was proposed to use the measured  $^7\text{Be}$  radioactivity with a Geographic Information System (GIS) to construct regional  $^7\text{Be}$  intensity fields for different altitude levels. From these intensity fields, the location of the  $^7\text{Be}$  source was determined. The second objective was to compare the time taken for the air masses from the  $^7\text{Be}$  source to Hong Kong with the experimentally determined residence times. Finally, the experimentally determined residence times were used together with the back-trajectories to locate the  $^7\text{Be}$  source.

## 2. Data and method

### 2.1. Air sampling

Hong Kong (22°18' N, 114°10' E) is a coastal city. The samples were collected 20 m above the ground on the roof of the Academic Building of the City University of Hong Kong. The samplings took place from November 2001 to February 2003.

The aerodynamic size distribution of  $^7\text{Be}$ -associated atmospheric aerosols was obtained using Sierra's Series 230 high-volume cascade impactors (Anderson 2000, Inc., Atlanta, GA, USA), which involved a flow rate of 68  $\text{m}^3 \text{h}^{-1}$  (or 40  $\text{ft}^3 \text{min}^{-1}$ ) and five atmospheric pressure stages for collecting aerosols larger than 0.49  $\mu\text{m}$ . The effective cutoff diameters of these impactors were 0.49, 0.95, 1.5, 3 and 7.2  $\mu\text{m}$ . Specially slotted glass-fiber filters were used to collect the aerosols on these stages. Another glass-fiber filter (without slots) used as a back-up filter was used to collect all aerosol particles with diameters below 0.49  $\mu\text{m}$ . Deposition of the particles in the glass-fiber lattice improved particle retention and reduced possible re-entrainment.

Sampling durations of exactly or very close to integral numbers of days were used in order to eliminate possible artifacts due to different sampling times. Time resolution varied from 1 to 4 d (23 h: 4 samples; 48 h: 63 samples; 49 h: 1 sample; 72 h: 2 samples; 96 h: 1 sample) and all of the readings were normalized to 48-h values (Yu and Lee, 2002). Immediately after collection, the glass-fiber filters (with or without slots) were folded and wrapped around the inner vertical surface of a 4-l Marinelli beaker, so that all filter papers had the same irradiation geometry to the germanium detector, for  $^7\text{Be}$  measurements using the high-resolution gamma-ray spectrometer.

### 2.2. Gamma-ray spectrometer and calibration

The  $^7\text{Be}$  intensities were measured using the area (number of counts) of the gamma peak at 477 keV in the gamma-ray spectra. The detector used was the EG&G ORTEC GMX90240 photon detector spectrometer system (EG&G ORTEC, Oak Ridge, TN). The type of cryostat configuration was Pop Top. The detector was an *n*-type coaxial high purity germanium crystal of 75.4 mm  $\times$  91.1 mm with a relative efficiency of 90%, which had a resolution of 2.18 keV at 1.33 MeV. The detector was placed inside a lead shield of 52 cm  $\times$  63.8 cm and 12 cm thickness. The uncertainties of the measurements of the gamma-ray spectrometer depended on the net counts as well as the background counts, and ranged from 260 to 1846 counts in our experiments. The ORTEC Gamma Vision for Windows A66-B32 version 5.1 software was used to control

the data acquisition and storage as well as the sample analysis and calibration.

### 2.3. Activity median aerodynamic diameter (AMAD) and residence time of $^7\text{Be}$ -associated aerosols

The aerosol-attached  $^7\text{Be}$  activity was approximated by a lognormal distribution. The AMAD and the geometric standard deviation (GSD) were conveniently determined by plotting the cumulative distributions on a piece of lognormal probability paper. In such a cumulative plot, the  $x$ -axis gave the logarithm of the aerodynamic diameter ( $D_p$ ) while the  $y$ -axis (in probit scale) indicated the cumulated percentage of  $^7\text{Be}$  activity (out of the total sum of  $^7\text{Be}$  activities on all stages) less than  $D_p$ .

If we plotted the inverse of a cumulative Gaussian distribution (expressed as probabilities in percentages) using a linear  $y$ -scale, we would get a sigmoidally shaped curve. Changing the  $y$ -scale to a (nonlinear) probability scale (ranging from 0.0001 to 99.999) could change the curve to appear as a straight line. The probit scale is similar to the probability scale, except that the scale is linear and the increment between tick marks is one standard deviation. The value “5” on the probit scale refers to the mean or 50% cumulative probability, while “6” refers to one standard deviation above the mean or 84.1% cumulative probability. Hence, the AMAD is obtained by the  $D_p$  value corresponding to the probit value of 5, and the GSD by the ratio of  $D_p$  values corresponding to probit values of 6 and 5.

After obtaining the AMAD for a particular sample, the residence time was estimated (Papastefanou and Ioannidou, 1995) by dividing the increase of the AMAD over the average size of the Aitken nuclei mode (i.e.,  $0.015\ \mu\text{m}$ ) by the mean growth rate (MGR) of  $0.004\text{--}0.005\ \mu\text{m h}^{-1}$  (McMurray and Wilson, 1982).

### 2.4. Back-trajectories plot and $^7\text{Be}$ intensity field

Three-dimensional 4-day back-trajectories were obtained every 3 h using the Hybrid Single-Particle Lagrangian Integrated Trajectory (HYSPLIT) model, which was produced by a joint effort between NOAA and Australia’s Bureau of Meteorology (web address: <http://www.arl.noaa.gov/ready/hysplit4.html>, NOAA Air Resources Laboratory, Silver Spring, MD). HYSPLIT is a system for computing simple air parcel trajectories to complex dispersion and deposition simulations. Gerasopoulos et al. (2001) commented that the use of back-trajectories for more than 3 d increased the uncertainty of the air-mass origin. However, as can be seen from the results below, the time taken for the  $^7\text{Be}$  to travel from the source to Hong Kong might need more than 3 d, so we relaxed the time constraint slightly to 4 d. We also studied the uncertainty of the air-mass

origin by using back-trajectories for more than 3 d in the section on Results and Discussion. Within a 48-h sampling period, there were 17 trajectories for each sample.

To construct a regional  $^7\text{Be}$  intensity field (cf. Gerasopoulos et al., 2001), we combined the  $^7\text{Be}$  intensity data with those of the 3-h end points of the back-trajectories, including the longitudes, latitudes and altitudes. Seibert et al. (1994) devised procedures to construct a “concentration field” for aerosols from their back-trajectories. The procedures developed here followed the idea outlined in Seibert et al. (1994), but modifications were introduced to take care of the different targets of investigation.

Seibert et al. (1994) transformed the concentration time series by taking the common logarithm before deducing the arithmetic mean since the aerosol concentration data were distributed approximately log-normally. However, Gerasopoulos et al. (2001) showed that the  $^7\text{Be}$  concentrations belong into two distinct classes represented by two Gaussian functions. With data for one of the stations studied, a bimodal distribution could not be statistically supported due to the lack of a sufficiently large amount of data. These were different from the aerosol concentration data investigated by Seibert et al. (1994). Therefore, in constructing the  $^7\text{Be}$  intensity field, logarithmic transformations were not performed.

Seibert et al. (1994) excluded the variations of aerosol concentrations introduced by the seasonal cycle of stability by using the sine and cosine waves with the period of 1 year determined by least-squares fitting. However, as can be seen in the following, the climate in Hong Kong is controlled by monsoons, so the prevailing wind directions are different in different seasons. In this way, the  $^7\text{Be}$  source regions are also different for different seasons. In the present investigation, we were interested in studying whether different  $^7\text{Be}$  source regions would have different  $^7\text{Be}$  intensities, so corrections for seasonal variations were not required or desired.

Seibert et al. (1994) used grid cells with a side length of about 150 km. The arithmetic mean for each grid cell was calculated using the residence time in the cell as a weighting factor, i.e.,

$$\bar{C}_{ij} = \frac{\sum_k C_k \tau_{ijk}}{\sum_k \tau_{ijk}}, \quad (1)$$

where  $i$  and  $j$  are indices of the grid ( $i, j$ ),  $\bar{C}_{ij}$  is the mean radionuclide concentration calculated for the grid,  $k$  represents a particular trajectory,  $\tau_{ijk}$  the time spent by the  $k$ th trajectory in the grid, and  $C_k$  is the radionuclide concentration value associated with the  $k$ th trajectory. However, in the present work, the HYSPLIT software does not provide information on  $\tau_{ijk}$ . However, it can be observed that  $\tau_{ijk}$  is inversely proportional to the mean

speed  $v_{ijk}$  of the air mass on the  $k$ th trajectory within and close to the grid  $(i,j)$ , which is in turn inversely proportional to the number  $N_{ijk}$  of fixed-time end points on the  $k$ th trajectory within a chosen area enclosing the grid  $(i,j)$ . In this way, the mean radionuclide concentration calculated for the grid could be alternatively given by

$$\bar{C}_{ij} = \frac{\sum_k C_k N_{ijk}}{\sum_k N_{ijk}}, \quad (2)$$

This was, in fact, just the value given by the average of the radionuclide concentrations of all fixed-time end points within the chosen area.

The  $^7\text{Be}$  intensity field was determined in the present work through Eq. (2) by employing a GIS. GIS can be used for integrating, analyzing, and displaying data which are spatially referenced to the Earth. The GIS softwares used in the present study were the ESRI ArcView 3.2a and its extension Spatial Analyst 2.0a.

All the data for the 3-h end points of the back-trajectories were first inputted into the system as point themes. By the “query” function, they were further divided into themes of four different altitude levels, namely, less than 1000, 1000–2000, 2000–3000 and above 3000 m (cf. Gerasopoulos et al., 2001). To construct the  $^7\text{Be}$  intensity field, the spatial distribution of  $^7\text{Be}$  intensities for each altitude level was needed, so the spatial relationship should be studied. The Spatial Analyst software is a tool for discovering and understanding spatial relationships in the data. The main component of the Spatial Analyst is the grid theme. The map is represented by equal-sized grids, each with a specific value of a certain attribute. In this study, the value of each grid was the mean  $^7\text{Be}$  intensity calculated from the end points surrounding the center point of the corresponding grid. The function of Neighborhood Analysis of the Spatial Analysis was adopted for this purpose. The mean  $^7\text{Be}$  intensities for each cell in the output grid theme were calculated using Neighborhood Statistics.

In this study, a grid theme of  $1^\circ \times 1^\circ$  square was built for each altitude level and the mean  $^7\text{Be}$  intensities were found from the 3-h end points within an area with radius of  $1.5^\circ$  from the centers of the cells.

### 3. Results and discussion

There was a total of 71 samples taken from November 2001 to February 2003, for which the  $^7\text{Be}$  intensities were measured and the AMAD of  $^7\text{Be}$ -associated atmospheric aerosols and thus the residence times were determined. The mean  $^7\text{Be}$  intensities for different months are shown in Table 1. From this table, we can see that high  $^7\text{Be}$  intensities were found in winter

Table 1  
Mean  $^7\text{Be}$  intensities normalized for 48 h for different months, with the ranges of AMAD and GSD also shown

Time	Mean $^7\text{Be}$ intensity (counts)	AMAD range ( $\mu\text{m}$ )	GSD range
Nov-01	1072	0.66–0.79	1.3–2.0
Dec-01	934	0.72–0.86	1.9–2.2
Jan-02	835	0.58–0.74	1.8–2.3
Feb-02	825	0.63–0.90	1.8–2.0
Mar-02	777	0.43–0.83	1.8–3.1
Apr-02	736	0.58–0.80	1.7–4.0
May-02	620	0.52–0.82	2.3–3.2
Jun-02	439	0.44–0.75	2.0–3.0
Jul-02	478	0.28–0.67	1.2–2.9
Aug-02	350	0.47–1.11	1.5–6.6
Oct-02	937	0.22–0.64	1.7–10.5
Nov-02	733	0.36–0.67	1.8–3.1
Dec-02	672	0.50–0.90	1.8–2.7
Jan-03	887	0.54–0.70	1.8–2.9
Feb-03	852	0.62–0.80	1.3–2.4

months, while low intensities were found in summer months. This result is in contrast to the finding of Feely et al. (1989) that  $^7\text{Be}$  concentrations at northern mid-latitudes showed a maximum in late summer. In Hong Kong, the spring months are from March to April; the summer months from May to August; the autumn months from September to October; and the winter months from November to February, each year.

The climate in Hong Kong is mainly controlled by monsoons. The summer months are dominated by the summer monsoon for which the warm and humid southwesterly wind prevails in South China and the South China Sea area including Hong Kong. The warm and damp marine air masses, which originate from the South China Sea, are carried to Hong Kong by the southwesterly winds. The winter months are governed by the winter monsoon for which the cold and dry northeasterly wind prevails in southern China and the South China Sea area. The cool and dry air masses, which originate from the Asian continent as far as Siberia, travel southeasterly over the Asian continent and the Yellow Sea to South Korea and southern Japan. These air masses then curve southwesterly across the East Sea and southeastern China to Hong Kong.

Our result that high  $^7\text{Be}$  intensities were found in winter months was in agreement with that of Takayuki et al. (1996), who showed that higher  $^7\text{Be}$  concentrations were found in winter and spring in Hakodate, which is situated in the northern part of Japan and is a place usually affected by the Siberian air mass during winter times. In relation to these results, it was, therefore, pertinent to determine whether the source of  $^7\text{Be}$  coincides with the source of the Siberian air mass.

Figs. 1(a–d) show the constructed regional  $^7\text{Be}$  intensity fields for altitudes less than 1000, 1000–2000, 2000–3000 and above 3000 m, respectively. From Fig. 1(a), we can see that low  $^7\text{Be}$  intensities were advected from low altitudes (less than 1000 m) and oceanic areas. The  $^7\text{Be}$  intensities increased for the higher intensity field layers. These results agree with the findings of Gerasopoulos et al. (2001). By examining Figs. 1(b–d), the  $^7\text{Be}$  source is likely situated in the northern part of Mongolia (see also the discussions below on the back-trajectory analyses using the experimentally determined residence times). It is well known that in winter, the land cools rapidly while cold, dense and heavy air masses are generated in the center of the Asian continent over northern Mongolia and southeastern Siberia to form an area of high atmospheric pressure, the Siberian anticyclone. The  $^7\text{Be}$  source identified here in the northern part of Mongolia is likely to be a result of STE exchange

and downward transfer in the troposphere. Surface winds around an anticyclone diverge away from the high-pressure center resulting in descending air, and anticyclonic conditions favor the downward mixing of higher  $^7\text{Be}$  radioactivities (Gerasopoulos et al., 2001).

Up to this point, only back-trajectories for 4 d were used. As mentioned before, Gerasopoulos et al. (2001) commented that the use of back-trajectories for more than 3 d increased the uncertainty of the air-mass origin. Now that the  $^7\text{Be}$  source was identified to situate at the northern part of Mongolia, attempt was made to examine the uncertainty of the air-mass origin by using back-trajectories for longer periods. The idea was to determine from the trajectories the time taken for an air mass to travel from the  $^7\text{Be}$  source to Hong Kong, which was then compared with the residence time determined from the AMAD of  $^7\text{Be}$ -associated atmospheric aerosols and the MGR of atmospheric aerosols. For the time

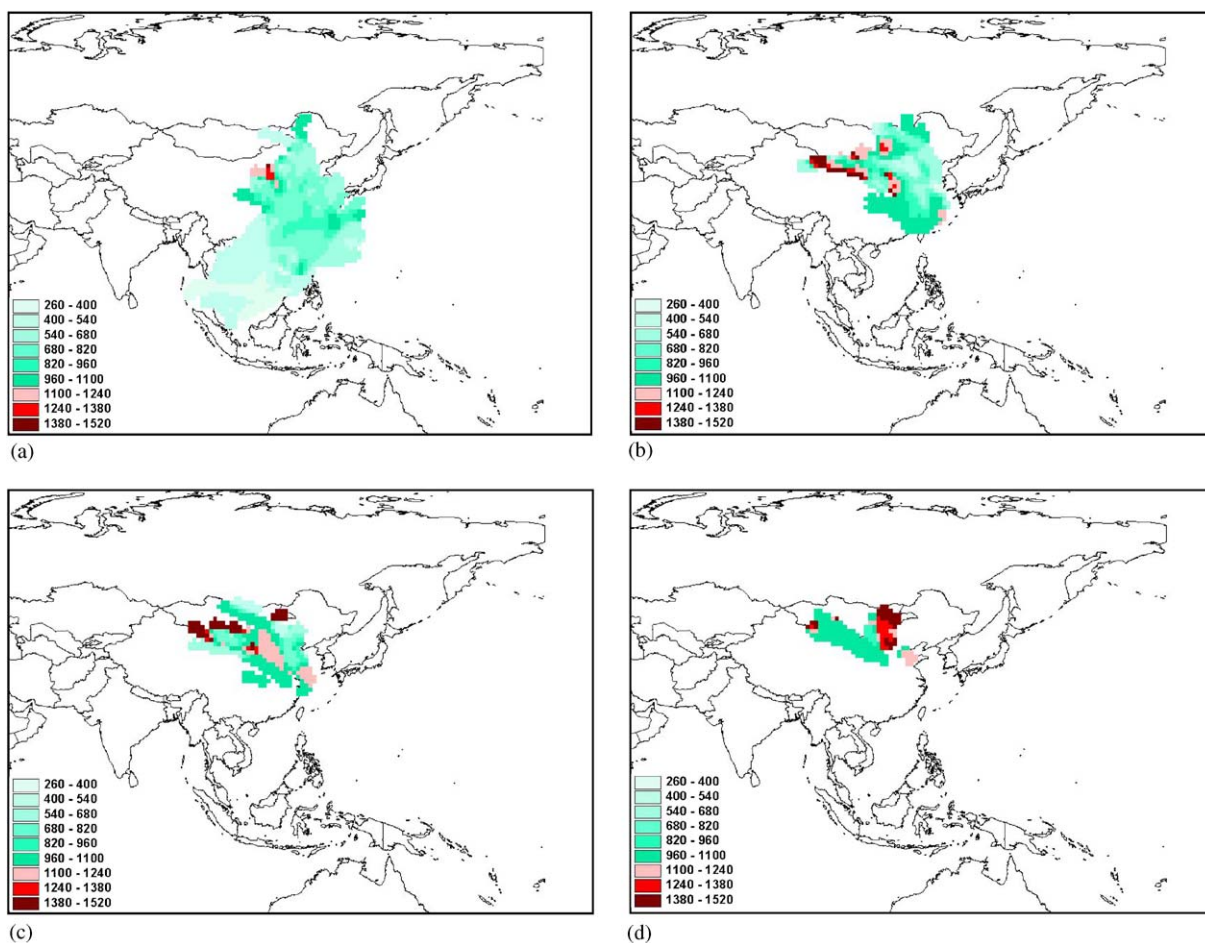


Fig. 1. (a) Regional  $^7\text{Be}$  intensity field for altitudes less than 1000 m. (b) Regional  $^7\text{Be}$  intensity field for altitudes 1000–2000 m. (c) Regional  $^7\text{Be}$  intensity field for altitudes 2000–3000 m. (d) Regional  $^7\text{Be}$  intensity field for altitudes above 3000 m.

being, the  $^7\text{Be}$  source was taken to be above 3 km and bound by the longitudes  $87^\circ 44'\text{E}$  and  $119^\circ 56'\text{E}$ , and latitudes  $41^\circ 35'\text{N}$  and  $52^\circ 09'\text{N}$ , which were the longitude and latitude ranges for Mongolia. Therefore, we went through all the 3-h endpoints which satisfied these criteria, and then determined the time taken for the corresponding air masses to come to Hong Kong.

Table 2 lists the time taken for air masses to come from the  $^7\text{Be}$  source to Hong Kong and the residence time determined from the AMAD of  $^7\text{Be}$ -associated atmospheric aerosols and the MGR of 0.004 and  $0.005\ \mu\text{m h}^{-1}$  for atmospheric aerosols (McMurray and Wilson, 1982). Good agreement was observed between the time taken to travel to Hong Kong and the residence time determined using the MGR of  $0.005\ \mu\text{m h}^{-1}$ . Taking into account the spread in the size of the Aitken nuclei mode, effects on particle sizes from factors such as wet precipitation (Röbig et al., 1980; Yu and Lee, 2002), uncertainties in the values of the determined AMAD, and that the area of the  $^7\text{Be}$  source was likely to extend beyond the north of Mongolia into southeastern Siberia (see discussions on the Siberian anticyclone above), the agreement can be regarded as excellent. This shows that for our investigation here, the use of back-trajectories was still satisfactory even up to 157 h (which is about 6.5 d).

With the justification of using back-trajectories to about 6 or 7 d, we can attempt to use the residence time determined from the AMAD of  $^7\text{Be}$ -associated atmospheric aerosols with the back-trajectories to locate the  $^7\text{Be}$  source. If the trajectory end point corresponding to the determined residence time was above 3000 m, we considered it to be within the  $^7\text{Be}$  source. All these end points in our samples corresponded to a travel time of less than 157 h by using the MGR of  $0.005\ \mu\text{m h}^{-1}$ , and are plotted in Fig. 2. The end points determined using the MGR of 0.004 and  $0.005\ \mu\text{m h}^{-1}$  are shown in blue circles and red triangles, respectively. We notice that the end points determined using the MGR =  $0.004\ \mu\text{m h}^{-1}$  are much more scattered, which agrees with the observation of results in Table 2 that MGR =

$0.005\ \mu\text{m h}^{-1}$  is more preferable. It is interesting to find that the end points determined using the MGR =  $0.005\ \mu\text{m h}^{-1}$  are relatively well confined in the areas of Mongolia and southeastern Siberia. This finding further supports that the  $^7\text{Be}$  source is associated with the Siberian anticyclone, and that some of the shorter times taken for air masses to come from the  $^7\text{Be}$  source to Hong Kong determined in Table 2 are due to the extension of the  $^7\text{Be}$  source beyond the north of Mongolia into the southeastern Siberia.

#### 4. Summary and conclusions

A total of 71  $^7\text{Be}$  samples were collected from November 2001 to February 2003 and measured using a high-efficiency germanium gamma-ray spectrometer. The total airborne  $^7\text{Be}$  radioactivities, the activity median aerodynamic diameter (AMAD) and the

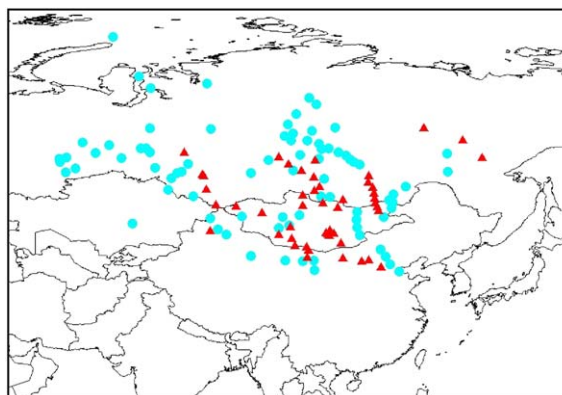


Fig. 2. Locations of  $^7\text{Be}$  sources with height above 3000 m determined using the residence time determined from the AMAD of  $^7\text{Be}$ -associated atmospheric aerosols with the back-trajectories. Blue circles: MGR =  $0.004\ \mu\text{m h}^{-1}$ ; red triangles: MGR =  $0.005\ \mu\text{m h}^{-1}$ .

Table 2

The time taken for air masses to come from the  $^7\text{Be}$  source to Hong Kong (HK) and the residence time determined from the AMAD of  $^7\text{Be}$ -associated atmospheric aerosols and the mean growth rate of 0.004 and  $0.005\ \mu\text{m h}^{-1}$  for atmospheric aerosols

Sample	Time taken to travel to HK (d)	Residence time (d) (calculated using MGR of $0.004\ \mu\text{m h}^{-1}$ )	Residence time (d) (calculated using MGR of $0.005\ \mu\text{m h}^{-1}$ )
020203	4.9–5.8	7.2	5.8
020306	4.4–4.9	7.3	5.8
020420	6.3–6.5	8.2	6.5
020426	5.0–5.0	6.3	5.0
021129	3.9–4.0	5.7	4.6
021213	3.5–4.7	5.8	4.7
021231	4.0–5.5	6.9	5.5
030119	3.7–4.8	6.0	4.8

residence times of  $^7\text{Be}$ -associated atmospheric aerosols were determined.

Procedures for constructing regional  $^7\text{Be}$  intensity fields were proposed. For each  $^7\text{Be}$  sample, by using the HYSPLIT model from NOAA Air Resources Laboratory, back-trajectories were obtained, to which the measured  $^7\text{Be}$  radioactivity was assigned. Grids of  $1^\circ \times 1^\circ$  square were employed, for which the mean  $^7\text{Be}$  intensities were found from the 3-h end points on the trajectories within an area with radius of  $1.5^\circ$  from the centers of the grids. No logarithmic transformation of the raw data and no correction for seasonal variations were required. The  $^7\text{Be}$  intensity fields showed that low  $^7\text{Be}$  intensities were advected from low altitudes (less than 1000 m) and oceanic areas, while higher  $^7\text{Be}$  intensities were associated with higher intensity field layers. An interesting finding here was the association of the  $^7\text{Be}$  source with the Siberian anticyclone.

The uncertainties of air-mass origins by using back-trajectories for more than 3 d were studied. By comparing the time taken for air masses to travel from the  $^7\text{Be}$  source to Hong Kong and the residence time determined from the AMAD of  $^7\text{Be}$ -associated atmospheric aerosols, good agreement was found if the mean growth rate of  $0.005 \mu\text{m h}^{-1}$  for atmospheric aerosols was used, and the use of back-trajectories was shown to be satisfactory even up to about 6.5 d.

Finally, the  $^7\text{Be}$  source was located using back-trajectories together with the residence times determined from the AMAD of  $^7\text{Be}$ -associated atmospheric aerosols. A trajectory end point corresponding to the determined residence time was considered to be within the  $^7\text{Be}$  source if it was above 3000 m. With a mean growth rate of  $0.005 \mu\text{m h}^{-1}$ , all these end points were relatively well confined in the areas of Mongolia and southeastern Siberia, which further supported that the  $^7\text{Be}$  source was associated with the Siberian anticyclone.

### Acknowledgements

We gratefully acknowledge the NOAA Air Resources Laboratory (ARL) for the provision of the HYSPLIT transport and dispersion model and/or READY website <http://www.arl.noaa.gov/ready.html> used in this publication.

### References

Al-Azmi, D., Sayed, A.M., Yatim, H.A., 2001. Variations in  $^7\text{Be}$  concentrations in the atmosphere of Kuwait during the period of 1994 to 1998. *Applied Radiation and Isotopes* 55, 413–417.

- Aldahan, A., Possnert, G., Vintersved, I., 2001. Atmospheric interactions at northern high latitudes from weekly  $^7\text{Be}$ -isotopes in surface air. *Applied Radiation and Isotopes* 54, 345–353.
- El-Hussein, A., Mohamemed, A., El-Hady, M.A., Ahmed, A.A., Ali, A.E., Barakat, A., 2001. Diurnal and seasonal variation of short-lived radon progeny concentration and atmospheric temporal variations of  $^{210}\text{Pb}$  and  $^7\text{Be}$  in Egypt. *Atmospheric Environment* 35, 4305–4313.
- Feely, H.W., Larsen, R.J., Sanderson, C.G., 1989. Factors that cause seasonal variations in Beryllium-7 concentrations in surface air. *Journal of Environmental Radioactivity* 9, 223–249.
- Gerasopoulos, E., Zanis, P., Stohl, A., Zerefos, C.S., Papastefanou, C., Ringer, W., Tobler, L., Hübener, S., Gäggele, H.W., Kanter, H.J., Tositti, L., Sandrini, S., 2001. A climatology of  $^7\text{Be}$  at four high-altitude stations at the Alps and the Northern Appennines. *Atmospheric Environment* 35, 6347–6360.
- Martell, E.A., 1970. Transport patterns and residence times for atmospheric trace constituents vs. altitude, In: *Radio-nuclides in the Environment, Advances in Chemistry Series*, vol. 93. American Chemical Society, Washington, DC, pp.138–157.
- McMurray, P.H., Wilson, J.C., 1982. Growth laws for the formation of secondary ambient aerosols: implications for chemical conversion mechanisms. *Atmospheric Environment* 16, 121–134.
- NRC, National Research Council, 1979. *Airborne Particles*. University Park Press, Baltimore, USA.
- Papastefanou, C., Ioannidou, A., Stoulos, S., Manolopoulou, M., 1995. Atmospheric deposition of cosmogenic  $^7\text{Be}$  and  $^{137}\text{Cs}$  from fallout of the Chernobyl accident. *The Science of the Total Environment* 170, 151–156.
- Papastefanou, C., Ioannidou, A., 1995. Aerodynamic size association of  $^7\text{Be}$  in ambient aerosols. *Journal of Environmental Radioactivity* 26, 273–282.
- Röbig, G., Becker, K.H., Hessin, A., Porstendörfer, J., Scheibel, H.G., 1980. A cascade impactor calibration for measurement of activity size distributions in the atmosphere. In *Proceedings of the Eighth Conference in Aerosol Science*, Georg-August-University. Göttingen, Germany, pp. 96–102.
- Seibert, P., Kromp-Kolb, H., Baltensperger, U., Jost, D.T., Schwikowski, 1994. Trajectory analysis of high-alpine air pollution data. In: Gryning, S.E., Milanm, M.M. (Eds.), *Air Pollution Modelling and Its Applications*, X. Plenum Press, New York, pp. 595–596.
- Stohl, A., Spichtinger-Rakowsky, N., Bonasoni, P., Feldmann, H., Memmesheimer, M., Scheel, H.E., Trickl, T., Hübener, S., Ringer, W., Mandl, M., 2000. The influence of stratospheric intrusions on alpine ozone concentrations. *Atmospheric Environment* 34, 1323–1354.
- Takayuki, T., Kenji, Y., Koh, H., Shizuo, T., 1996. Seasonal variations of residence time and upper atmospheric contribution of aerosols studied with  $\text{Pb-210}$ ,  $\text{Bi-210}$ ,  $\text{Po-210}$  and  $\text{Be-7}$ . *Tellus* 48 (B), 690–702.
- Talpos, S., Cuculeanu, V., 1997. A study of the vertical diffusion of  $^7\text{Be}$  in the atmosphere. *Journal of Environmental Radioactivity* 36, 93–106.

- Todorovic, D., Popovic, D., Djuric, G., 1999. Concentration measurements of  $^7\text{Be}$  and  $^{137}\text{Cs}$  in ground level air in the Belgrade city area. *Environmental International* 25, 59–66.
- Winkler, R., Dietl, F., Frank, G., Tschiersch, J., 1998. Temporal variation of  $^7\text{Be}$  and  $^{210}\text{Pb}$  size distributions in ambient aerosol. *Atmospheric Environment* 32, 983–991.
- Yu, K.N., Lee, L.Y.L., 2002. Measurements of atmospheric  $^7\text{Be}$  properties using high efficiency gamma spectroscopy. *Applied Radiation and Isotopes* 57, 941–946.